# Assessment of wood load condition by Near Infrared (NIR) spectroscopy

NICOLAS ANDRÉ*, NICOLE LABBÉ, TIMOTHY G. RIALS
*Tennessee Forest Products Center, The University of Tennessee, Knoxville, TN, USA*
*E-mail: nandre@utk.edu*

STEPHEN S. KELLEY
*National Renewable Energy Laboratory, Golden, CO, USA*

**Published online:** 17 February 2006

The assessment of the mechanical properties of wood using non-destructive evaluation (NDE) tools has been widely developed and refined. These NDE tools mainly rely on vibrational, ultrasonic or stress-wave approaches. Vibrational techniques generally show higher correlations between the estimated modulus of elasticity (MOE), or modulus of rupture (MOR), and the measured MOE, or MOR, than stress-wave techniques. They are, however, relatively difficult to apply in the field due to boundary conditions common in many timber structures. Thus, improved tools for assessing timber structures are still needed. Recently, near infrared (NIR) spectroscopy (500–2400 nm) has shown promise for predicting the MOE and MOR of wood. This work focuses on extending the use of NIR for measuring the load applied to small wood beams. The reflectance NIR spectrum was measured as the applied load was increased. Good correlations ($r > 0.96$) between the measured load and the predicted load were obtained using spectra taken from both the tension and compression surfaces of the small wood beams.


## 1. Introduction

Non Destructive Estimation has gained popular interest in the last decades. Through many different technical principles and experimental tools, NDE allows one to assess and monitor over time physical or mechanical properties of various materials, mainly steel (welding), concrete and solid wood. Moreover, recent materials such as wood-based composites, wood-plastic composites [1] rely or will rely on NDE to monitor their production (statistical process control, quality control, defects and foreign objects detection).

Tools that can be used for the nondestructive evaluation of simple beams or complex structures are common [2]. These methods can be used to evaluate the properties of a wood sample longitudinally (MOE and MOR) and transversely by correlating NDE and static measurements. Free vibrations [3] represent one means of estimating the modulus of elasticity (MOE) of a wood sample or a timber beam. The Fourier transform of the time signal recorded by an accelerometer is converted into a frequency signal that gives a vibratory modulus based on Bernoulli or Timoshenko formula [4]. Wang *et al.* [5] found a correlation coefficient (r) of 0.76 between stress-wave based dynamic MOE of piles and static MOE of small, clear wood samples (1 by 1 by 16 in.) extracted from these piles. In the same study, a correlation coefficient of 0.69 was found between the stress-wave based dynamic MOE of piles and static MOR of the small, clear wood samples. Values of the estimated mechanical properties and the corresponding correlation coefficients can vary greatly depending on the tool used (e.g., stress-wave, axial vibration, or bending vibration), the wood species, and the specimen size. As an illustration, Perstorper [3] found a correlation coefficient of 0.88 between the bending MOE and the static MOR for spruce beams ($70 \times 290 \times 5{,}800$ mm$^3$) using vibration techniques. For the same set of spruce beams, a correlation coefficient of 0.77 between the stress-wave based MOE and the static MOR was reported. Ceccotti *et al.* [6] found a correlation coefficient of 0.69 between axial vibration-based MOE and the static MOR for spruce beams ($80 \times 150$ mm$^2$). Larsson *et al.* [7] found a much stronger correlation ($r = 0.91$) between static MOE and bending vibration MOE for several spruce sets with different dimensions. Working with small-diameter logs (12

*Author to whom all correspondence should be addressed.
0022-2461 
DOI: 10.1007/s10853-006-4433-6

feet in length), Wang *et al.* [8] found correlations between the static MOE and transverse vibration MOE of approximately 0.77 and 0.92 for jack pine and red pine, respectively.

Correlations decrease with the quality of the tested wood sample. A study carried out by Galimard [9] showed weaker correlations between the static MOE and the NDE tools estimated MOE for a set of several hundred years old beams. Vibration based NDE tools gave the best correlations ($0.69 < r < 0.75$) between the estimated MOE and the static MOE compared to the stress-wave based tools ($0.49 < r < 0.58$). This study showed the tools' limitations when dealing with beams showing advanced decay and deep checks. In general, for simply supported beams, the bending vibration techniques provide a stronger correlation with static MOE than the stress-wave technique. However, as noted earlier, vibration techniques are fairly difficult to apply *in situ* to complex structures because of the boundary conditions.

Commercial products including Sylvatest [10], Pundit [10], CCT-4 [12], James V meter [13], Fakopp [14] and Metriguard 239A [15] have been developed based on these NDE techniques. Different commercial systems can be used for laboratory, manufacturing or field evaluations.

A second series of experiments point to the potential for measuring applied load with vibrational spectroscopy. Raman spectroscopy has been used to measure the applied load in synthetic and cellulose-based polymers and fibers. In particular, a series of papers by Eichhorn and coworkers [16–18], and others [19, 20] have highlighted the use of measuring shifts in the Raman spectral peaks as a function of applied load. These works demonstrated that Raman could be used to measure the load applied to natural and regenerated cellulose fibers. The magnitude of the Raman shift was highly dependent on the source of the cellulose, but generally a 2% strain (in tension) produced a 1–2 $cm^{-1}$ shift to lower frequencies. There was also a trend for a larger Raman shift for fibers with higher MOE. These results were explained by considering the deformation of bonds in the cellulose chain, as well as the reorientation of cellulose crystallites.

While Raman is very sensitive to these molecular scale changes, other spectroscopic tools are also of interest. Fourier Transform Infra Red (FT-IR), coupled with dynamic mechanical analysis (DMA) were used to stretch cellulose samples and record the infrared absorption of the OH-groups in the 3700–3000 $cm^{-1}$ region [21]. This broad overlapped band was divided into several distinct bands, demonstrating that FT-IR can detect the effect of an external mechanical perturbation on the molecular structure of the cellulose. Another study [22] carried by Hinterstoisser and coworkers used the same experimental setup in the 3950–700 $cm^{-1}$ range with celluloses from different origins to investigate the deformation behavior and its relation to molecular straining.

Near Infrared (NIR) spectroscopy is another non-destructive technique that has been successfully applied to predict mechanical properties of wood. Kelley et al. [23] used NIR spectroscopy to measure the chemical and mechanical properties of solid loblolly pine. Correlation coefficients of 0.88 were found for the MOE with the full spectral range (500–2400 nm) and with a reduced spectral range (650–1150 nm). Similar results have been obtained by Schimleck and coworkers [24], Meder and coworkers[25, 26], and others [27–29]. A related report by Kelley et al. [30] developed models of similar quality for predicting the mechanical properties of six different softwood species from NIR spectral data. This work also showed that the mechanical properties of the different species could be predicted from a single calibration model, as long as the model was developed with samples from all six of the species. Similar results were obtained for a model developed with spectra acquired from a softwood (pine) and a hardwood (aspen) [31].

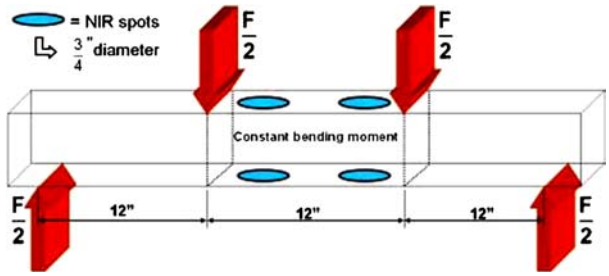


*Figure 1* Schematic of the four-point bending system used to measure the applied load and the NIR spectra.

With these background results, this work focused on demonstrating the use of NIR for measuring load applied to wood beams. NIR was selected since it has potential for being an inexpensive, portable, relatively durable tool that could be applied to wood beams in the field.

## 2. Materials and methods

Mechanical testing was carried out with a four-point bending geometry (Fig. 1) using three yellow poplar (*Poplas spp.*) specimens extracted from a dried board obtained in a local sawmill. This test configuration was selected because constant compression stresses are located on the upper face of the load span and constant tensile stresses are located on the bottom face of the load span. The applied load was well within the elastic domain of the beams as determined in preliminary tests on separate beams. The dimensions of the samples were 2″ by 2″ cross-section and 40″ length. A maximum load of 1,500 pounds was applied on each tested sample. The load was applied to the radial face of the sample at a rate of 0.3 in./min and monitored by a 50K lbs load cell.

NIR spectra were first collected without any load and then collected after each 50 pounds load increment. The NIR measurements were made with an Analytical Spectral Devices (ASD) Field Spectrometer at wavelengths between 500–2400 nm. A reflectance contact probe housing a high-intensity light source oriented at a right angle to the sample surface and a fiber optic oriented at 60 degrees to the sample surface was used to collect the reflectance

spectra. A piece of Spectralon® was used as a white reference material. For each NIR spot (0.75″ diameter), 10 scans were collected and averaged into a single spectrum. Four NIR spectra were collected at each 50 pounds increment, two on the compression zone (top fiber) and two in the tension zone (bottom fiber).

The reflectance spectra were transferred from the ASD to the Unscrambler® software (CAMO, Corvallis, OR). The reflectance spectra were converted to absorbance spectra and then normalized using routines in the Unscrambler®. Absorbance is related to reflectance by the following equation, where λ is the wavelength in nm: $A(\lambda) = \log(\frac{1}{R(\lambda)})$. Normalized spectra were submitted to multiplicative scatter correction (MSC) in order to remove scatter effects, which may be caused by surface roughness or subtle slope of grain, rather than true chemical or macromolecular differences. The data set was further reduced by averaging the spectra that were collected every 1 nm intervals, to a spectral data set at 5 nm intervals. The two spectra collected on the tension face for each load increment were averaged to one spectrum for each load increment, and the same process was used for the spectra collected in the compression face. Averaging the spectral data reduces the size of the spectra matrix and significantly reduces the time required to compute the Partial Least Squares (PLS) models without decreasing the quality of the models.

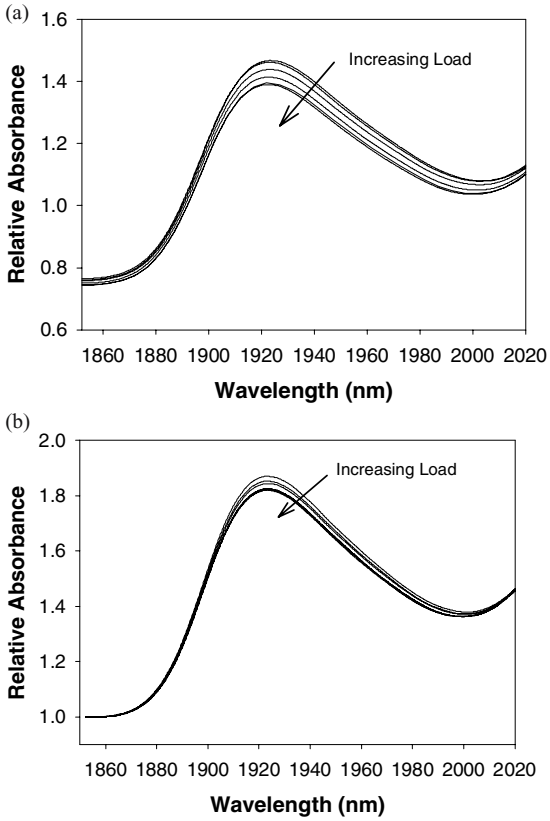


*Figure 3* Effect of the increasing load on the NIR spectra (1850–2020 nm) taken from the (a) tension face and (b) compression face.

## 3. Results and discussion

Fig. 2 shows four typical NIR spectra: a compression spectrum at 50 and 1500 pounds load, and the tension spectrum at 50 and 1,500 pounds load. Subtle differences can be observed between the tension and compression states and between a low and a high load.

Fig. 3a and b highlight the NIR spectra (1850–2020 nm) collected on the tension face and the compression face at 150 pound increments, respectively. Increasing the load decreases the absorbance at the longer wavelength providing a direct indication for the potential for measuring the load with NIR spectroscopy.

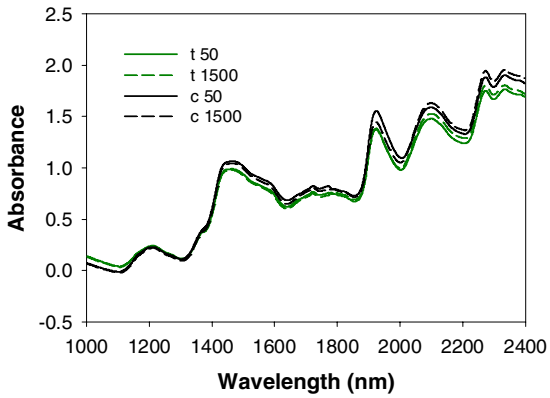


*Figure 2* Typical NIR spectra collected on the compression and tension faces (50 and 1,500 pounds) in the 1000–2400 nm region.

The vibration at 1924 nm has been assigned to interactions between cellulose hydroxyls and bound water [32, 33]. These changes in the NIR spectra are more subtle than those seen with Raman spectroscopy studies of cellulose fibers [16–18]. But this is not unexpected since the Raman vibrations are primary bond vibrations and these NIR vibrations are overtones. Also, the cellulose chains in these wood samples are supported by the hemicellulose-lignin matrix, which will also carry some of the applied load.

Principal component analysis (PCA) [34] was used to compare the tension/compression spectra. Not surprisingly there are two distinct clusters (Fig. 4), corresponding to the spectra collected on the compression face and those collected on the tension face.

These two clusters are identified by the first two principal components (e.g. PC1 and PC2). 77% of the total variance in the spectra is explained by the first principal component (PC1) and 17% is explained by the second principal component (PC2). This first principal component explains all the spectral differences due to tension or compression, while the second principal component can be attributed to spectral differences as a function of the applied load.

The chemical features (loadings) that differentiate the compression and tension faces are shown in Fig. 5. Fig. 5 also shows the original NIR spectra taken from the tension

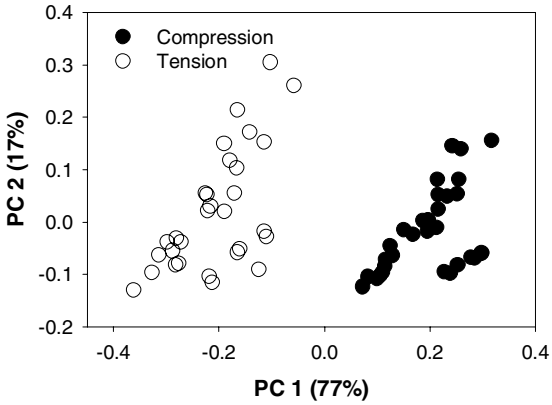


*Figure 4* Results from Principal Component Analysis (PCA) of the NIR spectra (1000–2400 nm) taken from both the compression and tension faces of the yellow poplar sample 3.

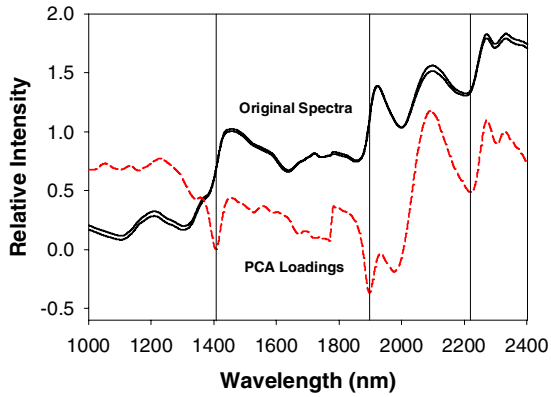


*Figure 5* Loadings from the PCA of the NIR spectra collected from the compression and tensions faces of yellow poplar 3. The original NIR spectra collected from the compression and tension faces of yellow poplar 3 subjected to an applied load of 1,500 pounds are also shown.

and compression faces of the sample loaded to 1,500 pounds.

As highlighted in Fig. 2, these original spectra are quite similar, but the PCA loadings show three sharp negative peaks at 1410, 1900, 2220 nm. All these peaks in the PCA loadings appear to be due to shifts in the cellulose hydroxyl vibrations at 1448, 1924, and 2270 nm, respectively [23]. The loadings for PC2 (not shown) appear to be due to relatively subtle spectral differences that can be attributed to the increased load on the samples.

Differences between the three individual samples can also be measured with PCA (Fig. 6). The results of PCA of the different samples (spectra from the tension face) show two clusters: sample 4 and samples 2 and 3. The PCA results for samples 2 and 3 are interspersed, which means that these two samples are similar in terms of their chemical composition and anatomical features, while sample 4 is somewhat different.

Nevertheless, the differences between the three samples are similar in magnitude to the differences caused by the application of the load. Based on the relatively large differences between the spectra taken from the compression face and tension face, and the relatively small

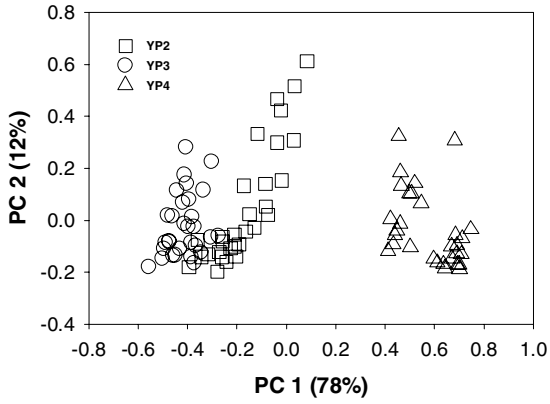


*Figure 6* Results from Principal Component Analysis (PCA) of the NIR spectra (1000–2400 nm) taken from the tension face of the yellow poplar samples 2, 3 and 4.

differences between the three different samples, the spectra taken from the compression and tension faces were used to predict the applied load and build the models for each individual sample and for all the samples together.

The NIR spectra taken from the tension face of YP2 were used to construct a PLS model [34] to predict the applied load (Fig. 7a). The PLS model shows the correlation between the measured load and the load predicted using the NIR spectra (1000–2400 nm). The CALB model constructed and this PLS model was then used to predict the applied load from the NIR spectra that were not included in the original model (VALD). There are very good correlations for both the CALB and VALD models ($r > 0.98$). The strong correlation for the VALD set is significant since these samples were not included in the original CALB model. The same approach was then used to construct a PLS model using the NIR spectra collected from the compression face (Fig. 7b).

As seen for the model from the spectra taken on the tension side of the sample, there is a very strong correlation between the measured load and the predicted load ($r > 0.97$). Again, the VALD set contained spectra that were not included in the original CALB model.

Based on the similarity between NIR spectra of all three samples (Fig. 6), PLS models were constructed using spectra from all three poplar samples. The PLS models constructed with the NIR spectra (1000–2400 nm) taken from the compression and tension faces are shown in Fig. 8a and b.

As seen with the models constructed with spectra from a single sample, there is a very strong correlation between the measured load and the predicted load using the NIR spectra. The correlations between the measured and predicted load are slightly lower for the models constructed from all three samples than those constructed from a single sample.

The overall trends and the effects of using different NIR spectral ranges are shown in Table I. All of these results are for the VALD set that was not included in the original PLS model. Reducing the spectral range from

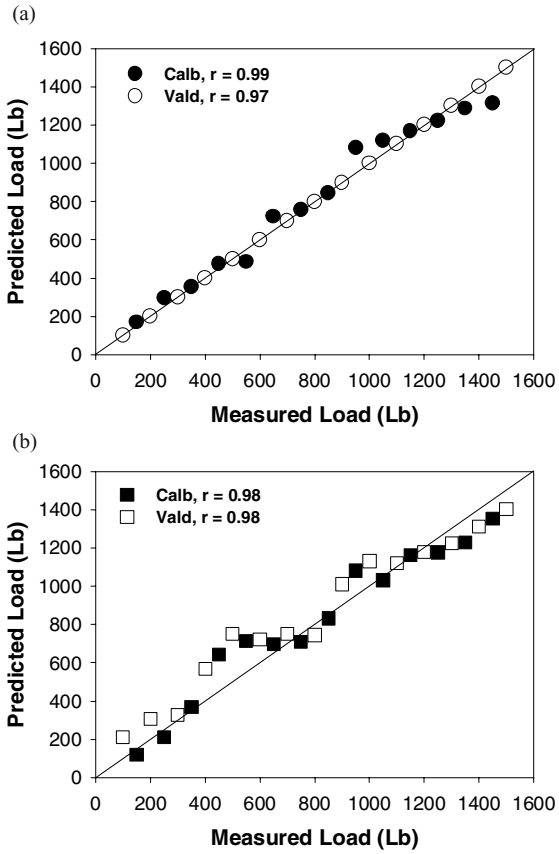


*Figure 7* Measured load and load predicted using NIR spectra (1000–2400 nm) taken from the (a) tension face and (b) compression face of yellow poplar 2.

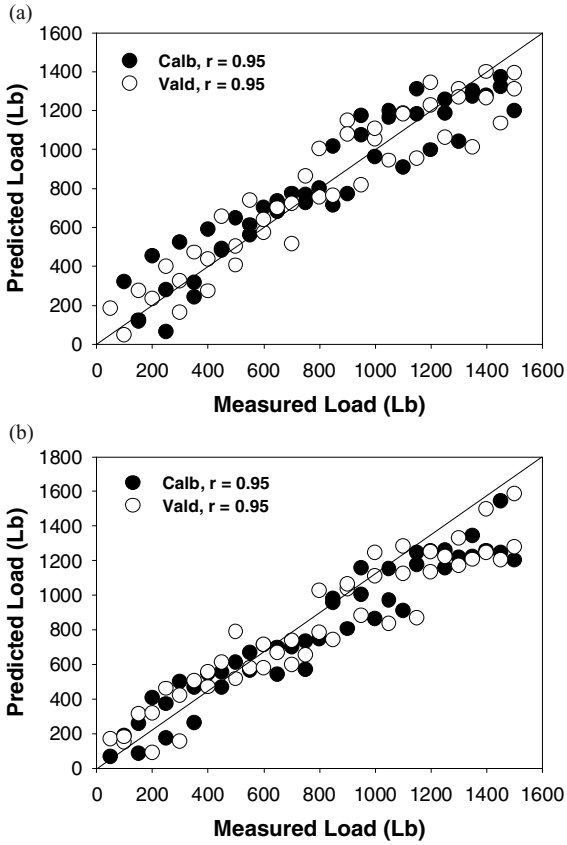


*Figure 8* Measured load and the load predicted using NIR spectra (1000–2400 nm) taken from the (a) tension face and (b) compression face of all three yellow poplar samples.

500–2400 nm, to 1000–2400 nm to 1850–2050 nm does not have significant negative impact on the quality of the models. The normalized root mean square error for prediction (RMSEP/average load) varies from 10 to 18% for the models for the single samples, and from 14 to 21% for the models for the all three combined samples.

Fig. 9a and b show the regression coefficients obtained from the PLS models computed on the NIR spectra from the tension and compression faces. The regression coefficients are the spectral features that are responsible for the correlation between the applied load and the load predicted from the NIR spectra [34].

It is clear that the regression coefficients for the tension and compression models are not the same. This is consistent with the PCA results (see Fig. 4) that show spectral differences for the tension and compression face of the samples. The multiple drawn rectangles, representing the most significant wavelengths as indicated by the Jack-Knifing function in Unscrambler®, emphasize differences between tension and compression. The Jack-Knifing function [35] relies on uncertainty tests performed on the PLS model parameters. Useless or unreliable parameters may be eliminated. Student's t-tests are performed for each regression coefficient and its estimated variance found during the cross-validation process (subsets within all the spectral data are created to calibrate models that are then validated on the remaining data) at a given significance level (usually at a 95% confidence interval).

There are three major sets of vibrations that drive the correlation between the measured and predicted applied load for spectra collected from both, the tension face (1180–1280 nm, 1780–1846 nm and 2170–2290 nm) and the compression face (1390–1508 nm, 1632–1710 nm, and 1892–1982 nm). This analysis suggests that the chemical groups that are changing with the applied load are different for tension and compression, which is consistent with the PCA results in Fig. 4. The origin of these differences could be found in the wood structure itself. Wood is a very complex composite material consisting of fibers composed of cellulose embedded in a matrix of lignin and hemicellulose. The nanostructure of a fiber cell wall shows an arrangement of multiple layers (Primary, S1, S2 and S3) of different thicknesses that have fractions of the main chemical compounds [36]. Cellulose is found in the microfibrils which reinforce the hemicellulose-lignin matrix. The S2 layer, which is the thickest (about 40 times thicker than the others), is reinforced by microfibrils that lie from 5 to 30 degrees to the longitudinal axis. This layer plays a major role in supporting the weight of the tree and the tension and compression forces generated by the wind. Its microfibril angle (MFA) has a direct impact on the axial modulus of elasticity (low MFA values mean high MOE

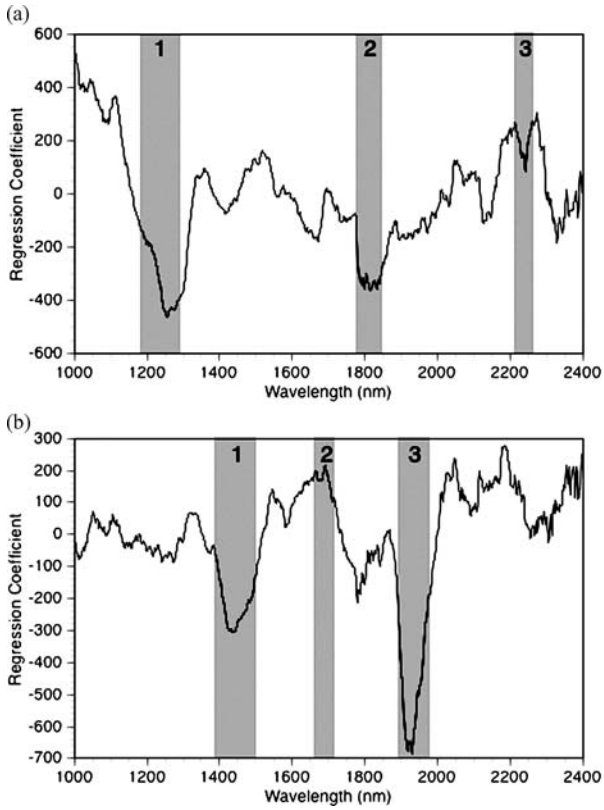


*Figure 9* Regression coefficients from the PLS regression of the NIR spectra collected from the (a) tension face and (b) compression face of all three yellow poplar samples.

values). Wood cell walls have been compared with reinforced concrete: cellulose microfibrils (CMF) would be the steel rods, the hemicellulose-lignin matrix would be the concrete [37]. This analogy could explain for some of the differences seen in the regression coefficients of the PLS models for the tension and the compression faces. Microfibrils (cellulose) could be more solicited when tension forces occur while the hemicellulose-lignin matrix could play a more important role when compression forces occur. Assignments of NIR vibrations to specific wood components have been provided by a number of authors including work by Fourty and coworkers [32], Ali and coworkers [33], Tsuchikawa and coworkers [38], among others. Using these assignments, the vibrations that are significant contributors to the PLS models for tension and compression can be made. The vibrations that are significant for the compression model include overtones for crystalline and amorphous OH in cellulose (between 1390–1508 nm), CH first overtones (1632–1710 nm) in lignin, and cellulose OH and water (between 1892–1982 nm). The first set of vibrations is represented by negative regression coefficients (negative peak), the second set by a positive peak and the third set by a strong negative peak (Fig. 9b). By associating the assigned peaks with their corresponding signs, we could state that, when the load increases, cellulose is less solicited (1st and 3rd sets with negative peaks) and lignin is more solicited (2nd set with a positive peak). This would be in accordance with the theory of the reinforced concrete. In the case of the model for the tension face, significant vibrations include CH second and first overtones (between 1180–1280 nm, and 1780–1846 nm, respectively) for both cellulose and lignin, and a combination of CH and CC double bonds vibrations in lignin (between 2170–2290 nm). The first set of vibrations is represented by negative regression coefficients (strong negative peak), the second set by a negative peak and the third set by a positive peak (Fig. 9a). It not possible to draw any conclusion for the tension face because two out of the three main peaks are assigned to both cellulose and lignin. As these two peaks are negative, it would be convenient to state that they are in fact related to lignin and not cellulose.

TABLE I The correlation coefficient and normalized root mean squared error of prediction (Norm. RMSEP) for PLS models constructed using different samples and wavelength ranges

| | 500–2400 nm | | 1000–2400 nm | | 1850–2050 nm | |
|---|---|---|---|---|---|---|
| Dataset | r | Norm. RMSEP | r | Norm. RMSEP | r | Norm. RMSEP |
| YP2 Comp. | 0.98 | 0.12 | 0.98 | 0.14 | 0.97 | 0.16 |
| YP2 Ten. | 0.97 | 0.13 | 0.97 | 0.12 | 0.99 | 0.10 |
| YP3 Comp. | 0.99 | 0.09 | 0.97 | 0.14 | 0.98 | 0.12 |
| YP3 Ten. | 0.99 | 0.10 | 0.98 | 0.12 | 0.98 | 0.10 |
| YP4 Comp. | 0.96 | 0.17 | 0.97 | 0.14 | 0.98 | 0.11 |
| YP4 Ten. | 0.95 | 0.18 | 0.97 | 0.14 | 0.97 | 0.13 |
| All YP Comp. | 0.97 | 0.14 | 0.95 | 0.18 | 0.92 | 0.21 |
| All YP Ten. | 0.96 | 0.16 | 0.95 | 0.18 | 0.94 | 0.19 |

All these models are constructed with an independent set of samples that were not used in the original model. All of the PLS models for the single samples used 2 or 3 latent variables (loadings) and those for the combined samples used 4 or 5

Tsuchikawa et al. [38] monitored the diffusion of deuterium oxide ($D_2O$) in Sitka spruce by FT-NIR spectroscopy. They observed significant intensity reduction at 1380–1630 nm and 2000–2220 nm and assigned these bands to the first overtone of the fundamental OH stretching vibration of cellulose and to a combination band of the OH and CH deformation modes, respectively. By working with the second derivative of the NIR spectra in the 1380–1630 nm region, they assigned more specifically some overlapped bands to the amorphous (1420 nm), "semi-crystalline" (1490 nm) and crystalline (1550 and 1590 nm) regions of the cellulose. PLS models constructed using vibrations between 1380–1630 nm and 2000–2220 nm for both the tension and compression faces had correlation coefficients above 0.9, only slightly less than models that used the entire spectral region of 1000–2400 nm or the vibrations highlighted by Jack-Knifing. This clearly shows that the high modulus cellulose is very sensitive to load variations in both tension and compression.

Prior work has shown that high quality PLS models for stiffness and ultimate strength can be constructed with a variety of different wood species and there are several examples of high quality models that can predict the

properties of several different species [30, 31]. These same trends could be seen for NIR models for applied load. This could allow the development of NIR hardware and software that would be used to predict the applied load for a variety of wood species in different service environments. NIR has already been used to predict the mechanical properties of wood with varying moisture contents [39], decayed wood [40] and creosote treated wood [41]. Thus, the use of NIR tools to make measurements in a variety of environments has great potential.

## 4. Conclusion

Until now, NIR spectroscopy has been used to predict mechanical properties (MOE and MOR) of solid wood from spectra collected from either solid or grounded wood. In this study, three yellow poplar samples were tested in bending while collecting NIR reflectance spectra on their compression and tension faces. It has been demonstrated that NIR spectroscopy coupled to PLS analyses can be used to predict tension or compression loads within these wood samples. Strong correlations ($r > 0.95$) were found for each individual sample tested and also for all the samples together. These strong correlations provide experts with a new tool to monitor and diagnose timber structures. The regression coefficients obtained from the PLS model for the tension face (all samples together) were different than the ones obtained from the PLS model for the compression face. A parallel was drawn for the compression face between the main compounds identified from the regression coefficients and those involved in the reinforced concrete theory. Yet, it was not possible to draw the same parallel for the tension face due to the presence of chemical groups belonging to both cellulose and lignin.

## 5. Acknowledgments

The authors would like to thank Dr. Richard Bennett and Randy Rainwater (The University of Tennessee, Department of Civil and Environmental Engineering) for providing the four-point bending apparatus and the LVDT used to measure the samples' displacements. This work was supported with funds from a USDA, Wood Utilization Research Program.

## References

1. B. J. TUCKER and D. A. BENDER, *Forst Prod. J.* **53**(6) (2003) 27.
2. R. J. ROSS and R. F. PELLERIN, USDA, Forest Service, Forest Product Laboratory, General Technical Report FPL-GTR-70, Madison, Wisconsin, USA (1981) p. 27.
3. M. PERSTORPER, in Proceedings of the 1st European Symposium on Nondestructive Evaluation of Wood, Sopron, Hungary, September 1994, pp. 321–330.
4. O. ALDRAIHEM, R. WETHERHOLD and T. SINGH, *J. Int. Mat. Syst. Struct.* **8**(2) (1997) 149.
5. X. WANG, R. J. ROSS, J. R. ERICKSON, J. W. FORSMAN, G. D. MCGINNIS and R.C. DE GROOT, Research Note FPL-RN-0274, USDA, Forest Service, Forest Product Lab. (2000) p. 11.
6. A. CECCOTTI, T. NAKAI and M. TOGNI, in Proceedings of the 1st European Symposium on Nondestructive Evaluation of Wood, Sopron, Hungary, (1994) p. 443.
7. D. LARSSON, S. OHLSSON and M. PERSTORPER, in Proceedings of the IUFRO S5.02 Timber Engineering Meeting, Köpenhamn, Denmark, (1997) p. 11.
8. X. WANG, R. J. ROSS, J. A. MATTSON, J. R. ERICKSON, J. W. FORSMAN, E. A. GESKE and M. A. WEHR, *Forest Pro. J.* **52**(2) 2002 79.
9. P. GALIMARD, Convention DERF # 61.45.19/00 Report, 2001, 14 p. (unpublished).
10. J. L. SANDOZ, in Proceedings of the 1st European Symposium on Nondestructive Evaluation of Wood, Sopron, Hungary, (1994) p. 216
11. J. S. MACHADO, R. SARDINHA and H. CRUZ, in Proceedings of the 5th World Conference on Timber Engineering, Montreux, Switzerland, (1998) p. 304.
12. P. KUKLIK and J. DOLEJS, in Proceedings of the 5th World Conference on Timber Engineering, Montreux, Switzerland, (1998) p. 692.
13. W. W. WILCOX, *Forest Prod. J.* **38**(5) (1988) 68.
14. F. DIVOS, L. NEMETH and L. BEJO, in Proceedings of the 11th International Symposium on Nondestructive Testing of Wood, Madison, Wisconsin, USA, (1999) p. 153.
15. R. J. HOYLE and R. F. PELLERIN, in Proceedings of the 4th Symposium on Nondestructive Testing of Wood, Vancouver, Washington, USA, (1978) p. 33.
16. S. J. EICHHORN, M. HUGHES, R. SNELL and L. MOTT, *J. Mater. Sci. Lett.* **19** (2001) 721.
17. S. J. EICHHORN, R. J. YOUNG, R. J. DAVIES and C. RIEKEL, *Polym.* **44** (2003) 5901.
18. S. J. EICHHORN and R. J. YOUNG, *Comp. Sci. Tech.* **63** (2003) 1225.
19. W. T. Y. TZE, Ph.D. dissertation. University of Maine, Orono, ME, USA, (2003) p. 191.
20. F. DADASHIAN and M. A. WILDING, *Ind. J. Fib. Tex. Res.* **28** (2003) 385.
21. B. HINTERSTOISSER and L. SALMÉN, *Vibr. Spectro.* **22** (2000) 111.
22. B. HINTERSTOISSER, M. ÅKERHOLM and L. SALMÉN, *Biomacromolecules* **4**(5) (2003) 1232.
23. S. S. KELLEY, T. G. RIALS, R. SNELL, L. H. GROOM and A. SLUTER, *Wood Sci. Tech.* **38**(4) (2004) 257.
24. L. R. SCHIMLECK, R. EVANS and J. ILIC, *Canadian J. Forest Res.* **31**(10) (2001) 1671.
25. A. THUMM and R. MEDER, *J. Near Infrared Spectro.* **9**(2) (2001) 117.
26. R. MEDER, A. THUMM and H. BIER, *Holz als Roh- und Werkstoff* **60**(3) (2002) 159.
27. W. GINDL, A. TEISCHINGER, M. SCHWANNINGER and B. HINTERSTOISSER, *J. Near Infrared Spectros.* **9**(4) (2001) 255.
28. J. B. HAUKSSON, G. BERGQVIST, U. BERGSTEN, M. SJOSTROM and U. EDLUND, *Wood Sci. Tech.* **35**(6) (2001) 475.
29. P. HOFFMEYER and J. PEDERSEN, *Holz als Roh- und Werkstoff* **53** (1995) 165.
30. S. S. KELLEY, T. G. RIALS, L. R. GROOM and C-L. SO, *Holzforschung* **58**(3) (2004) 252.
31. L. R. SCHIMLECK, R. EVANS and J. ILIC, *IAWA J.* **22**(4) (2001) 415.
32. T. FOURTY, F. BARET, S. JACQUEMOUD, G. SCHMUCK and J. VERDEBOUT, *Remote Sens. Environ.* **56** (1996) 104.
33. M. ALI, A. EMSLEY, H. HERMAN and R. HEYWOOD, *Polym.* **42**(7) (2001) 2893.
34. H. MARTENS and T. NÆS, in *Multivariate Calibration* (John Wiley & Sons, 1989) 419.
35. K. H. ESBENSEN, in *Multivariate Data Analysis—In Practice* (CAMO Process AS, 2001) 598.
36. R. E. BOOKER and J. SELL, *Holz als Roh- und Werkstoff* **56**(1) (1998) 1.

37. R. E. MARK in *Cell Wall Mechanics of Tracheids* (Yale University Press, 1967) 310.
38. S. TSUCHIKAWA and H. W. SIESLER, *Applied Spectroscopy* **57**(6) (2003) 667.
39. R. R. MEGLEN and S. S. KELLEY, US Patent 6,525,319, 2003.
40. S. S. KELLEY, U.S. Patent 6,593,572, (2003).
41. S. E. II HEDRICK, Master's Thesis, The University of Tennessee, Knoxville, TN, USA (2003) p. 49.

*Received 3 May*
*and accepted 20 June 2005*